High Linearity and High Efficiency of Class-B Power Amplifiers in GaN HEMT Technology

Vamsi Paidi, Shouxuan Xie, *Student Member, IEEE*, Robert Coffie, Brendan Moran, Sten Heikman, Stacia Keller, Alessandro Chini, Steven P. DenBaars, *Member, IEEE*, Umesh K. Mishra, *Fellow, IEEE*, Stephen Long, *Senior Member, IEEE*, and Mark J. W. Rodwell, *Senior Member, IEEE*

***Abstract*—A 36-dBm high-linearity single-ended common-source class-B monolithic-microwave integrated-circuit power amplifier is reported in GaN high electron-mobility transistor technology. We also describe the design and simulation of highly linear and highly efficient common-source and common-drain class-B power amplifiers. Single-ended class-B amplifiers with bandpass filtering have equivalent efficiency and linearity to push–pull configurations. The common-source class-B circuit demonstrates high linearity, greater than 35 dBc of third-order intermodulation (IM3) suppression and high power-added efficiency (PAE) of 34%. Simulations of common-drain class-B designs predict a PAE of 54% with a superior IM3 suppression of more than 45 dBc over a wider range of bias due to the strong series–series negative feedback offered by the load resistance.**

***Index Terms*—GaN high electron-mobility transistor (HEMT), high linearity, intermodulation suppression, monolithic-microwave integrated-circuit (MMIC) power amplifiers.**

I. Introduction

MODERN communications networks require efficient power amplifiers with low distortion. Class-A amplifiers exhibit low distortion, but exhibit power-added efficiency (PAE) well below 50% [1]. Improved efficiency is obtained with switched-mode amplifiers [2], [3]. These, unfortunately, exhibit high intermodulation distortion (IMD) in multitone applications. Push–pull class-B amplifiers offer the potential for improved efficiency, at a theoretical limit of 78.6%, combined with distortion as low as class A.

For operation in sub-octave bandwidths, a classical push–pull class-B power amplifier can be replaced by a single-ended class-B power amplifier together with a low-pass or band-pass filter. The single-ended class-B power amplifier can achieve high PAE and high third-order intermodulation (IM3) suppression simultaneously if the drain current ($I_{\rm d}$) versus gate-to-source voltage ($V_{\rm gs}$) characteristic is linear above threshold. It is also shown that common-drain class B has low distortion and the distortion is much less sensitive to biasing conditions than similar common-source configurations.

Manuscript received September 30, 2002. This work was supported by the Office of Naval Research under ONR Class D/E Contract N00014-00-1-0653.

V. Paidi, S. Xie, R. Coffie, S. Heikman, S. Keller, A. Chini, U. K. Mishra, S. Long, and M. J. W. Rodwell are with the Electrical and Computer Engineering Department, University of California at Santa Barbara, Santa Barbara, CA 93106 USA (e-mail: paidi@ece.ucsb.edu).

B. Moran and S. P. DenBaars are with the Materials Department, University of California at Santa Barbara, Santa Barbara, CA 93106 USA.

Digital Object Identifier 10.1109/TMTT.2002.807682

The gallium–nitride material system is a leading contender for microwave wireless applications due to its superior electrical properties. The high electron velocity ($>10^7$cm/s), wide bandgap (3.4 eV), and high breakdown voltage ($>$50 V for a current gain cutoff frequency f_T of 50 GHz) of the AlGaN/GaN system result in record power densities. The high thermal conductivity (3.5 W/cm $\cdot$ K) of SiC substrates significantly reduces thermal limitations, leading to power density as high as 11.2 W/mm [4].

Previous work in GaN-based circuits [5]–[7] has demonstrated broad-band amplification in class-A topology with good linearity. Efficient and linear amplification is necessary to make this material system useful in the competitive field of RF power amplifiers. This paper investigates class-B amplifier design and fabrication with the objective of gaining high efficiency coupled with low distortion. Several key points should be now noted regarding efficiency and linearity as a function of amplifier bias point (class A versus classes B and C).

First, unlike class-A amplifiers, class-B and class-C amplifiers do not dissipate power when input signals are not present. This is a key advantage in transmitters where signals of strong amplitude or pulse modulation are present. Second, at moderate power levels, approaching, but below the amplifier 1-dB compression point ($P_{1\,\rm dB}$), a class-B amplifier shows higher PAE than class A. Finally, when class-A amplifiers are operated at output power levels well beyond the 1-dB gain compression point, the device is driven strongly into both cutoff and saturation on the peaks of the signal swing, and PAE can substantially exceed the theoretical 50% PAE limit of linear unsaturated class-A amplification. These points are relevant to amplifier linearity. In class-B operation, at power levels well below $P_{1\,\rm dB}$, it is expected that the distortion is increased relative to that of class A as a result of device switching. This is the penalty incurred for increased PAE. At power levels approaching or beyond $P_{1\,\rm dB}$, in both classes A and B, the devices are driven into saturation, and substantial distortion is generated. Such high-distortion operation is not acceptable in many RF and microwave systems, and the amplifier has to be operated at power levels below $P_{1\,\rm dB}$.

II. Push–Pull Configuration

Push–pull common-drain class B is popular in the audio power amplifier design [8]. In fact, the usage of push–pull dates back to the age of vacuum tubes [9]. Complementary devices or transformers are necessary for push–pull operation [10]. Efficient broad-band class-B amplification is unfortunately not

feasible at microwave frequencies due to the lack of available baluns with the required zero ohm *even-mode* impedance [11].

Push–pull cancels even-order distortion by means of symmetry [11]. The push–pull configuration takes an exact replica of the single device transfer function and creates an image about the current (Y) axis and subtracts it from the original transfer function. If the transfer function of a single device is

$$I_o = f(V_{\rm in}) = I_{\rm dc} + I_1 \cdot V_{\rm in} + I_2 \cdot V_{\rm in}^2 + I_3 \cdot V_{\rm in}^3 + I_4 \cdot V_{\rm in}^4 + \cdots \quad (1)$$

then with push–pull, the total transfer function becomes

$$I_o = f(V_{\rm in}) - f(-V_{\rm in}) = 2 \cdot I_1 \cdot V_{\rm in} + 2 \cdot I_3 \cdot V_{\rm in}^3 + \cdots. \quad (2)$$

We must emphasize that push–pull operation, through its symmetry, suppresses only even-order (second harmonic) distortion [see Fig. 1(a)]. Odd-order components in the circuit transfer function and the resulting two-tone third-order IMD are not suppressed.

Efficient class B requires significant drain currents at even harmonic frequencies in order to realize the ideal half-sinusoidal drain current waveform. For example, at the class-B conduction angle of 180°, the second harmonic current is $4/(3\pi)$ times the fundamental current to achieve this condition. A balun that presents high impedance at even harmonics, as is the case for Marchand, Lange, and Wilkinson baluns, do not provide an even-mode short circuit. This is in marked contrast to the situation at radio frequencies, where ferrite-loaded baluns provide the required even-mode impedance. The permeability of most ferrites is, however, low at microwave frequencies. Therefore, efficiency will be degraded. In addition, microwave baluns are physically large (of the order of $\lambda/2$), which results in both large excess consumed integrated circuit (IC) die area and in large-excess line losses with resulting further degradation in efficiency.

III. Single-Ended Class-B Power Amplifier

Let us consider the effect of bandpass filtering on the transfer function of a single device. Any function can be written as a sum of an even and odd function, as shown in Fig. 1(b), and as follows:

$$I_o = f(V_{\rm in}) = \left(\frac{1}{2}\right) \cdot \big(f(V_{\rm in}) + f(-V_{\rm in})\big) + \left(\frac{1}{2}\right) \cdot \big(f(V_{\rm in}) - f(-V_{\rm in})\big). \quad (3)$$

The even part consists of the dc term and the even powers of $V_{\rm in}$, and the odd part consists of the odd powers of $V_{\rm in}$ as follows:

$$\left(\frac{1}{2}\right) \cdot \big(f(V_{\rm in}) + f(-V_{\rm in})\big) = I_{\rm dc} + I_2 \cdot V_{\rm in}^2 + I_4 \cdot V_{\rm in}^4 + \cdots \quad (4)$$

$$\left(\frac{1}{2}\right) \cdot \big(f(V_{\rm in}) - f(-V_{\rm in})\big) = I_1 \cdot V_{\rm in} + I_3 \cdot V_{\rm in}^3 + \cdots. \quad (5)$$

The even part of the transfer function creates harmonic frequency content and even-order IMDs, which are removed by the bandpass filter. The odd part creates in-band IMDs, which cannot be filtered. However, the filter removes the harmonic distortion caused by the odd components of the transfer function.

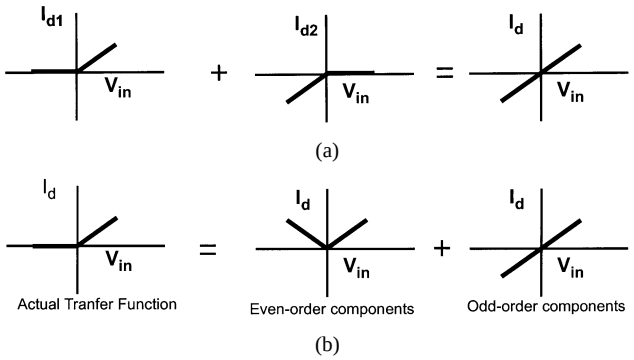

Fig. 1. Graphical analysis and comparison of push–pull and single-ended configurations. (a) Graphical representation of push–pull. (b) Even and odd part of a single-ended transfer function.

Third-order in-band IMD characteristics of class-B push–pull circuits, therefore, do not differ from that of a single-ended class-B amplifier. Consequently, for power-amplifier applications requiring less than 2 : 1 frequency coverage, push–pull operation is entirely unnecessary. Instead, all harmonic Fourier components of the transistor drain current waveform can be supplied (provided with the required low impedance) through use of an output bandpass filter, centered at the signal fundamental, and a single transistor stage can be employed. Drain voltage harmonic distortion is likewise suppressed by the low impedance at harmonic frequencies presented by the output filter. IM3 characteristics are identical for both push–pull and single-ended configurations. Therefore, given an operating bandwidth requirement of less than an octave, a single-ended class-B amplifier can provide both high linearity and drain efficiency approaching 78.6%.

IV. Common-Source Class-B Amplifier

Two-tone third-order distortion characteristics depend critically upon the class-B bias point, whether for single-ended or for the equivalent push–pull configuration. Bias design is, however, most easily discussed in the framework of the push–pull stage. With drain current $I_{\rm d}(V_{\rm in})$, the push–pull output current is

$$I_o = I_{\rm d}(V_{\rm in}) - I_{\rm d}(-V_{\rm in}). \quad (6)$$

The circuit diagram and transfer function of the push–pull common-source class-B amplifier are shown in Fig. 2. An ideal push–pull power amplifier is assumed and the transfer function is observed as a function of the bias voltage starting from class-C bias to class-A bias. The class-C bias has a range of input voltage for which neither of the devices is on. This nonlinearity causes crossover distortion. At class-B bias, there is no crossover distortion, and if the transfer function of the device is linear above threshold, the net transfer function also becomes linear. At class-AB bias, the two devices will be simultaneously on for part of the signal cycle. In this case, if the transfer function is linear above threshold, circuit gain is doubled for that portion of the transfer function in which both devices are on. Distortion is, therefore, generated. Finally, for

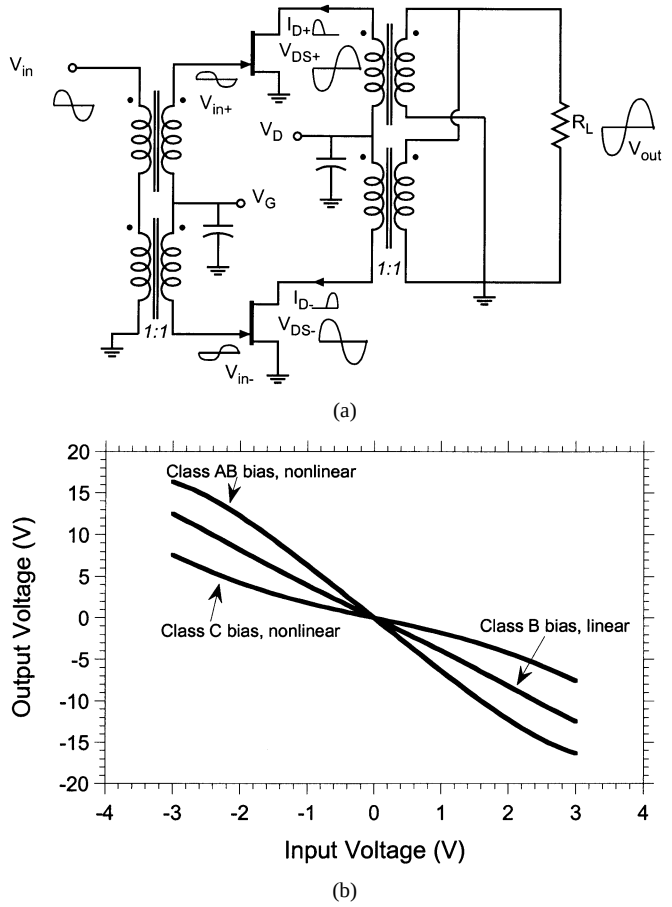

Fig. 2. Transfer characteristics of a push–pull common-source class-B power amplifier. (a) Schematic of push–pull common-source amplifier. (b) Voltage transfer function under different bias conditions.

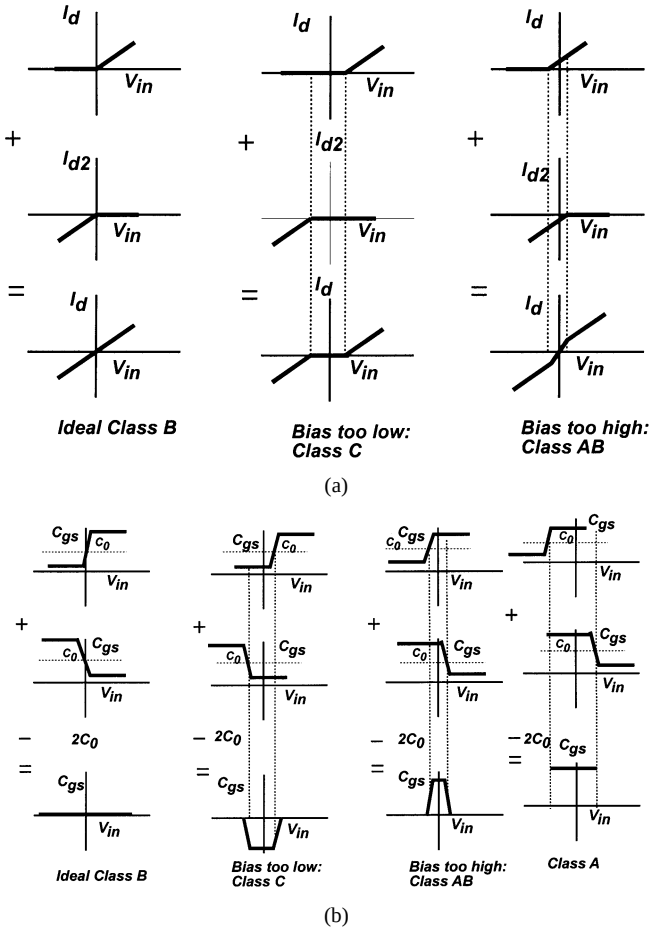

Fig. 3. Bias design for common-source class-B power amplifier. (a) $I_{\rm d}$ versus $V_{\rm gs}$ nonlinearity. (b) The even-part (except C_0) of $C_{\rm gs}$ characteristic.

class-A bias, both devices will be on simultaneously over the entire signal cycle. Hence, the transconductance will be twice of a single device, and the transfer function will be linear, provided that the device has constant g_m above threshold. Class B can, therefore, provide both high efficiency and moderately low distortion. The distortion of class B is very sensitive to the specific slope of $I_{\rm d}$–$V_{\rm gs}$ characteristic, particularly near threshold. The arguments above are graphically described in Fig. 3(a).

In the above discussion, distortion due to voltage variable input capacitance $C_{\rm gs}$ was neglected. For signal frequencies larger than approximately current gain cutoff frequency $(f_t)/10$, the distortion due to input capacitance variation can be comparable to that arising from the g_m variation above threshold. The nonlinearity in the gate charge and, therefore, input capacitance, introduces distortion in the gate voltage waveform. The third-order charge term contributes to the in-band IMD. The charge stored in $C_{\rm gs}$ can be expressed as

$$Q = q_0 + q_1 V + q_2 V^2 + q_3 V^3 + \cdots. \tag{7}$$

The gate current is then

$$i = \frac{\partial Q}{\partial t} = q_1 \frac{\partial V}{\partial t} + 2q_2 V \frac{\partial V}{\partial t} + 3q_3 V^2 \frac{\partial V}{\partial t} + \cdots. \tag{8}$$

By definition

$$\begin{aligned} C(V) &= \frac{\partial Q}{\partial V} = q_1 + 2q_2 V + 3q_3 V^2 + \cdots \\ &= c_0 + c_1 V + c_2 V^2 + \cdots. \end{aligned} \tag{9}$$

Hence, the gate current is

$$i = c_0 \frac{\partial V}{\partial t} + c_1 V \frac{\partial V}{\partial t} + c_2 V^2 \frac{\partial V}{\partial t} + \cdots = C(V) \frac{\partial V}{\partial t}. \tag{10}$$

The second-order coefficient c_2 in $C(V)$ contributes to in-band third-order IMD through $c_2 V^2(\partial V/\partial t)$, while the fourth-order coefficient c_4 contributes to in-band IM3 through $c_4 V^4(\partial V/\partial t)$. In general, all even-order terms in (9) contribute to in-band IMD, and should be compensated or cancelled for best linearity. Zero IM3 requires that the even components $C_{\rm gs,\,even}$ be zero as follows:

$$\begin{aligned} C_{\rm gs,\,even} &= c_2 V^2 + c_4 V^4 + \cdots \\ &= \left(\left(\frac{1}{2} \right) \cdot \left(C_{\rm gs}(V_{\rm in}) + C_{\rm gs}(-V_{\rm in}) \right) \right) - c_0. \end{aligned} \tag{11}$$

Experimental data of GaN high electron-mobility transistors (HEMTs) exhibit a $C_{\rm gs}(V_{\rm gs})$, which is very nearly antisymmetric about $V_{\rm gs} = V_{\rm th}$. In this case, biasing the devices at class B results in minimum $C_{\rm gs,\,even}$, and minimum resulting

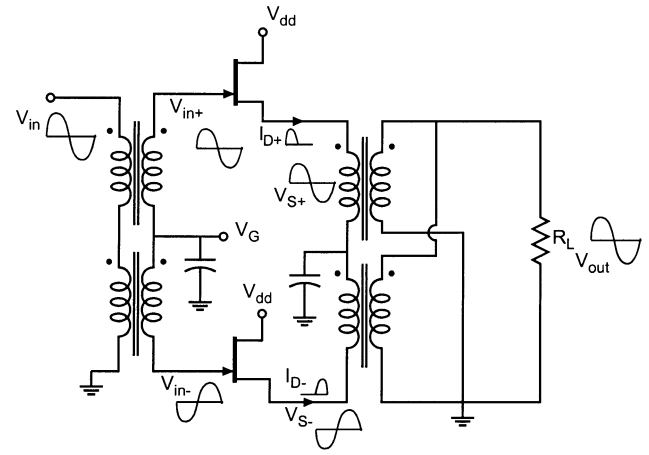

(a)

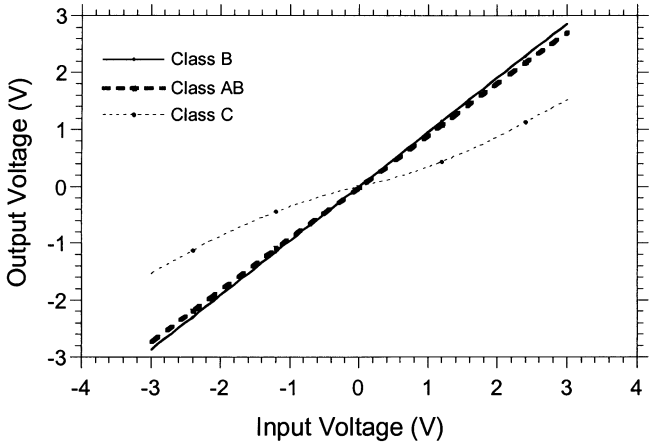

(b)

Fig. 4. Transfer characteristics of a push–pull common-drain class-B power amplifier. (a) Schematic of push–pull common-drain amplifier. (b) Voltage transfer function under different bias conditions.

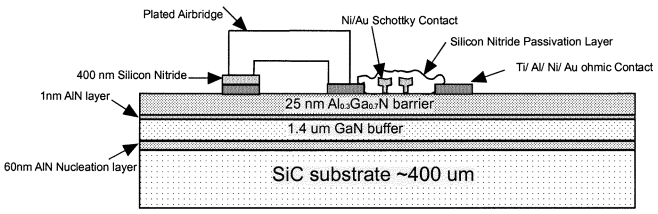

Fig. 5. Wafer cross section showing the MMIC process of GaN HEMT technology on an SiC substrate.

IM3. This is shown graphically in Fig. 3(b) for different bias conditions. If biased at class B, the even-order components of $C_{\rm gs}$ are small due to the antisymmetric characteristics of the $C_{\rm gs}$ about the pinchoff voltage. When biased slightly above threshold (class AB), the $C_{\rm gs}$ characteristic has significant even-order components that contribute to the distortion in the gate voltage waveform with resulting degradation in the distortion. In class-A operation, however, the input capacitance is almost constant over the signal swing and the distortion is low. Once again, to the extent to which $C_{\rm gs}$ is antisymmetric about the device threshold, distortion is suppressed by biasing the device at threshold, e.g., class-B bias.

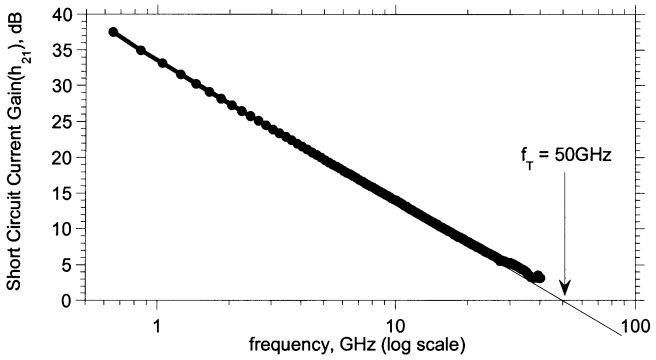

Fig. 6. Current gain cutoff frequency (f_t) of 0.25 × 150 μm^2 single-gate device at $V_{\rm gs} = -3.5$ V, $V_{\rm ds} = 15$ V.

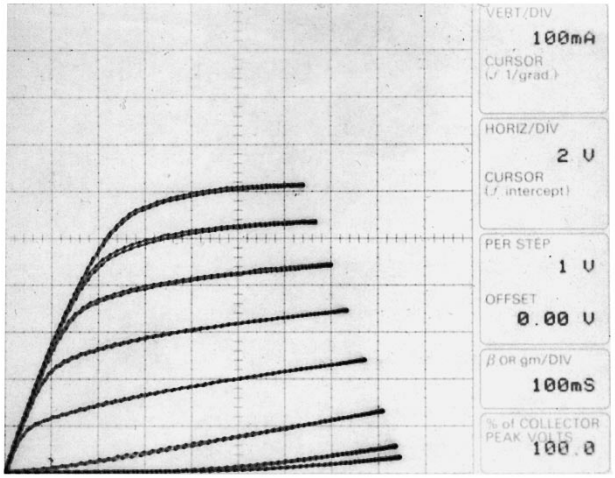

Fig. 7. Pulsed $I_{\rm d}$-versus-$V_{\rm gs}$ (80-μs pulsewidth) superimposed on dc characteristics of a 600-μm single-gate GaN HEMT.

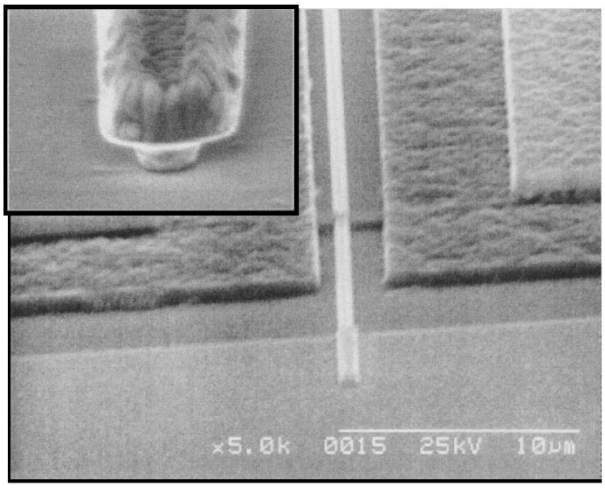

Fig. 8. SEM figure of a typical single-gate GaN HEMT (inset shows T-gate).

V. Common-Drain Class-B Amplifier

Bipolar implementation of the push–pull common collector class-AB amplifier is the most widely used topology in the audio regime. The HEMT equivalent, the common-drain amplifier,

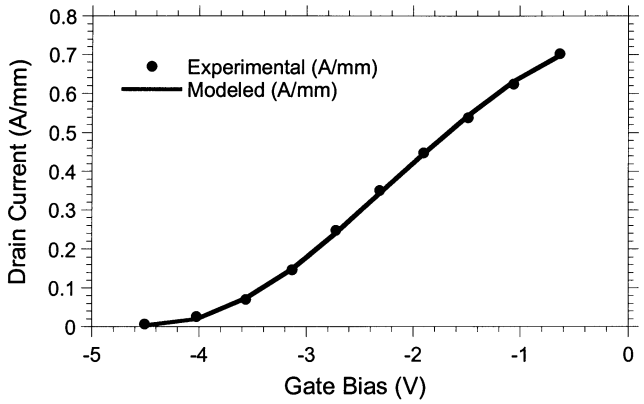

(a)

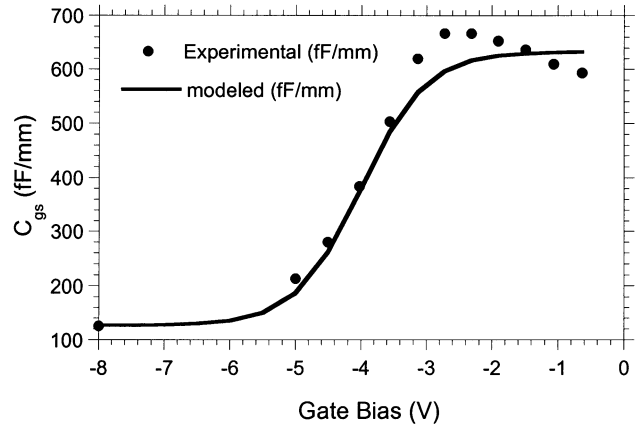

(b)

Fig. 9. Modeling of the transconductance and input capacitance characteristics. (a) Fitting of $I_{\rm d}$–$V_{\rm gs}$ characteristic of GaN HEMT on SiC. (b) Fitting of $C_{\rm gs}$ as a function of $V_{\rm gs}$.

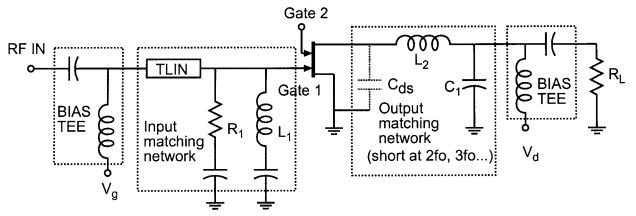

Fig. 10. Circuit diagram of common-source class-B power amplifier.

has the potential to become a linear amplifier with good efficiency, when biased at or above class B. For common-source class B, the transfer function is

$$\frac{\partial V_{\rm out}}{\partial V_{\rm in}} = -R_{\rm Load} \cdot g_m(V_{\rm gs}). \tag{12}$$

Voltage variation in the transconductance $g_m(V_{\rm gs})$ directly produces nonlinearity of the net transfer function. However, for the common-drain configuration, the transfer function is

$$\frac{\partial V_{\rm out}}{\partial V_{\rm in}} = \frac{R_{\rm Load} \cdot g_m(V_{\rm gs})}{1 + R_{\rm Load} \cdot g_m(V_{\rm gs})}. \tag{13}$$

As g_m is made large in comparison with the conductance of the load ($R_{\rm Load} \cdot g_m \gg 1$), the effect of transconductance variation $g_m(V_{\rm gs})$ on circuit gain is reduced. The strong series–series negative feedback presented by the load linearizes

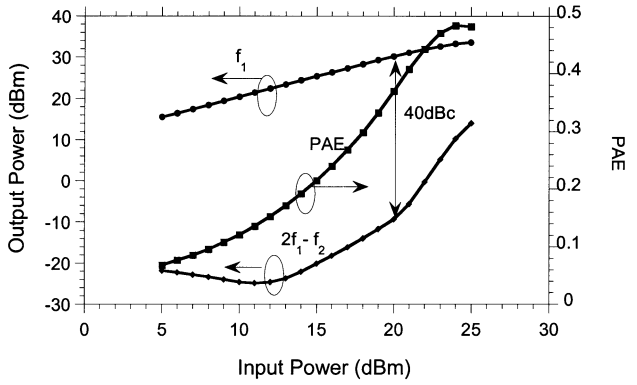

Fig. 11. Simulation of common-source class-B power amplifier at 10 GHz. PAE is for single-tone operation, while the output power curves are for two-tone operation.

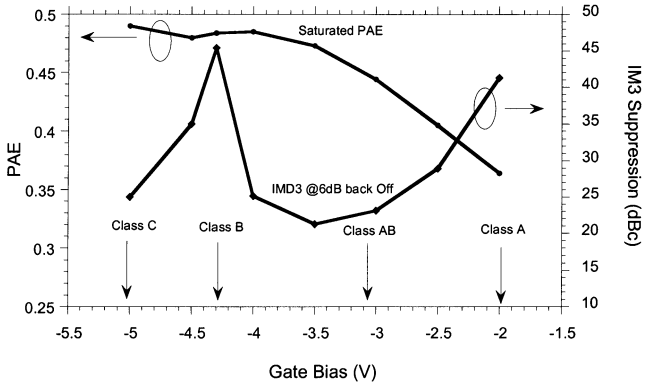

Fig. 12. Simulation of common-source class-B power amplifier: single-tone PAE, two-tone IM3 suppression at 10 GHz as a function of bias.

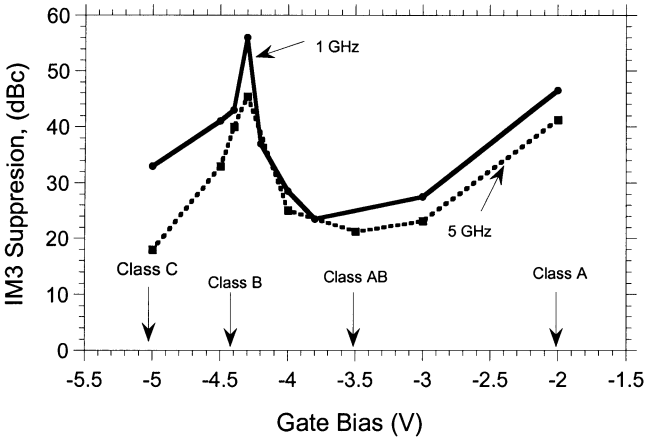

Fig. 13. Simulation of common-source class-B power amplifier: two-tone IM3 suppression at 1 GHz, 5 GHz as a function of bias.

the amplifier. The linearity is most directly analyzed in the framework of the push–pull configuration. Single-ended operation with an octave bandpass filter is, once again, equivalent to push–pull. The circuit diagram and transfer function at various bias conditions are shown in Fig. 4(a) and (b), respectively. The transfer function is nonlinear at class-C bias ($V_{\rm gs} < V_{\rm th}$ under bias), as neither of the devices is on for part of any given cycle. As class-B bias conditions ($V_{\rm gs} = V_{\rm th}$ under bias) are approached, the distortion improves rapidly.

The circuit exhibits low distortion even at class-AB bias and improves further as the bias is increased into class-A operation ($I_{\rm d} = I_{\max}/2$ under bias). Even if the $I_{\rm d}$-versus-$V_{\rm gs}$ transfer function is nonlinear above threshold, this configuration effectively reduces distortion when biased at class AB.

The above static transfer function analysis does not include the effect of nonlinear parasitic input capacitance, an effect that increases distortion significantly for frequencies greater than $f_t/10$.

VI. Device Performance and Process Technology

A. Process

A nine-mask-level monolithic-microwave integrated-circuit (MMIC) process is used in the fabrication of the power amplifiers. The wafers are grown on a 400-μm-thick SiC substrate, using metal organic chemical vapor deposition (MOCVD). The HEMT layer structure and fabrication process are shown in Fig. 5. The Ti(20 nm)/Al(150 nm)/Ni(37.5 nm)/Au(50 nm) ohmic contacts to the channel are e-beam evaporated and then annealed at 870 °C for 30 s in forming gas ambient. Device mesas are etched using Cl_2-based reactive ion etching. The gates with a T-profile are written using a bilayer electron-beam lithography process. The gate length is approximately 0.25 μm. The gate Schottky metal contact is Ni(30 nm)/Au(270 nm).

80-nm silicon nitride (Si_3N_4) is deposited using plasma-enhanced chemical vapor deposition (PECVD) to passivate the high field regions of the devices. This passivation layer plays a crucial role in reducing the long-time constant charge storage in surface states and enhancing the high-frequency large-signal power gain. A second 400-nm PECVD Si_3N_4 layer is used for the dielectric in the metal–insulator–metal (MIM) capacitors (0.13 fF/μm^2). The plated airbridges interconnect the HEMT source contacts and bridge ground planes in the coplanar waveguide transmission lines.

B. Performance

Devices with 150-μm gate peripheries exhibit 50 GHz of f_t (Fig. 6). The pulsed $I_{\rm d}$-versus-$V_{\rm ds}$ characteristics of a 600-μm single-gate device at 80-μs pulse duration are shown superimposed on the dc characteristics of the device in Fig. 7. $V_{\rm gs}$ is pulsed from the pinchoff voltage to the required bias, while $V_{\rm ds}$ is held constant. This process is repeated for $V_{\rm ds}$ starting from 16 to 0 V. The traces are so close to each other as to be hard to distinguish. This indicates minimal dc–RF dispersion, and is indicative of successful passivation. The image of a typical single-gate GaN HEMT is shown in Fig. 8.

VII. Modeling

The Curtice C_FET3 model[1] is used to model GaN HEMTs in Agilent ADS RF simulation software. The small-signal S-parameters of the device are measured sweeping a wide range of frequency from 50 MHz to 40 GHz. The extrinsic parameters are extracted by measuring the small-signal S-parameters for the open and short structures of the device. The intrinsic parameters are then obtained by deembedding the extrinsic parameters. From the measurements, the bias dependence of the intrinsic parameters ($C_{\rm gs}$, $I_{\rm d}(V_{\rm gs})$, $g_m(V_{\rm gs})$) are determined.

[1]W. R. Curtice, Curtice Consulting, Washington Crossing, PA.

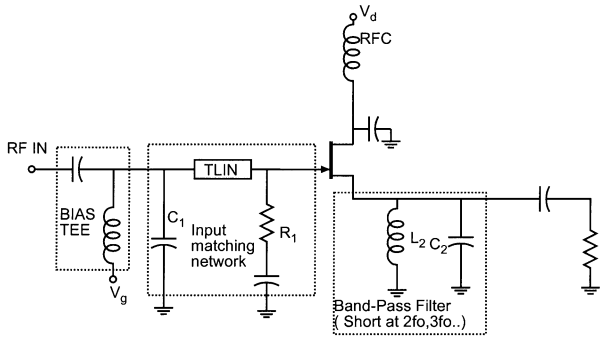

Fig. 14. Circuit diagram of common-drain class-B power amplifier.

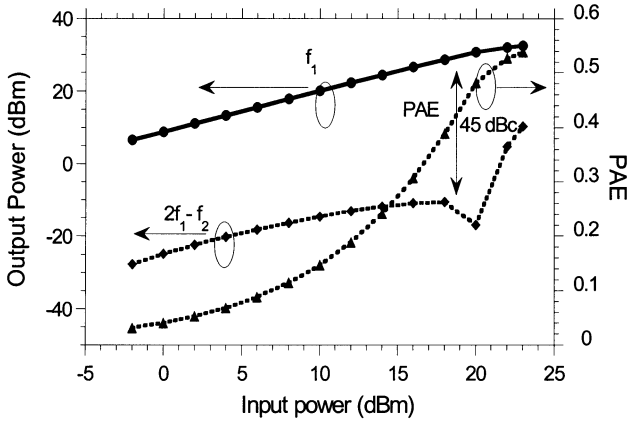

Fig. 15. Simulated performance of common-drain class-B bias at 10 GHz. PAE is for single-tone operation, while the output power curves are for two-tone operation.

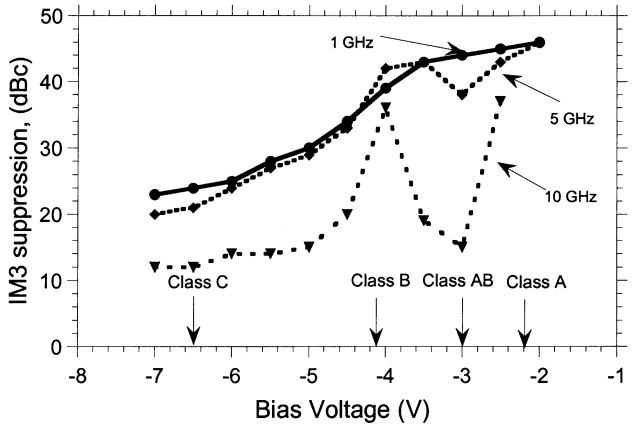

Fig. 16. Simulations of common-drain class B: two-tone IM3 suppression at 1, 5, and 10 GHz.

Designs have been developed for the University of California at Santa Barbara's (UCSB's) GaN HEMT MMIC process. Designs were developed using the model of a 0.25-μm gate-length (L_g) device, resulting in 50-GHz f_t [12] and 100-GHz power-gain cutoff frequency, $f_{\max}$. The devices have 50-V breakdown and the saturation current ($I_{\rm dss}$) is 650 mA/mm. These device parameters are representative of better GaN HEMTs fabricated at UCSB. The I–V characteristics are fitted by a third-order polynomial [see Fig. 9(a)],

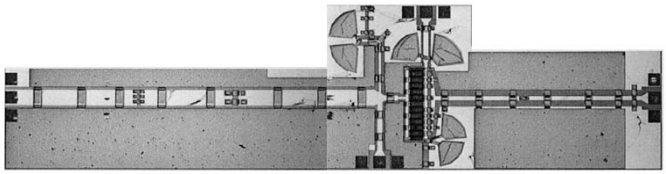

Fig. 17. Chip photograph of GaN HEMT MMIC power amplifier (dimensions: 6 mm × 1.5 mm).

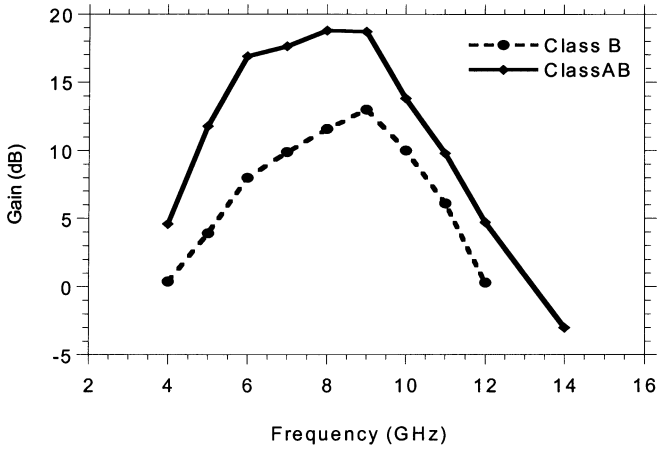

Fig. 18. Measured power gain versus frequency for a GaN MMIC.

and the bias dependence of the intrinsic input capacitance ($C_{\rm gs}$) is fitted by a hyperbolic tangent function [see Fig. 9(b)]. Transconductance and input capacitance are the key parameters in the linearity analysis. Note that the measured device shows $C_{\rm gs}(V_{\rm gs})$ deviating significantly from the modeled curve that is perfectly antisymmetric about $V_{\rm th}$.

VIII. Simulations of Common-Source Class B

The input is matched at 10 GHz, and the output is tuned to present low impedance for the harmonic frequencies. The drain–source capacitance $C_{\rm ds}$ is absorbed into the output π section for higher bandwidth and optimum load-line matching. The circuit diagram and the PAE simulations are shown in Figs. 10 and 11. The circuit uses a GaN HEMT with 1.2-mm channel width, and it produces 48% of saturated PAE with 36 dBm of output power at 10 GHz. Two-tone simulation ($2f_1$–f_2) predicts 40 dBc of IM3 suppression when the total output power is 3 dB below the 1-dB compression point. The bias has been varied from class-C to class-A bias, and the IMD performance along with PAE are plotted in Fig. 12. From these simulations, it can be inferred that class-B bias achieves optimum results with regard to both efficiency and linearity. The distortion degrades very rapidly on either side of the class-B bias, confirming the theoretical predictions. At lower frequencies, the linearity is improved and follows the same trend (Fig. 13).

IX. Simulations of Common-Drain Class B

The circuit diagram of a common-drain class-B amplifier is shown in Fig. 14. A lossy input-matching network is required to ensure stability. A bandpass *LC* tank circuit at the output short

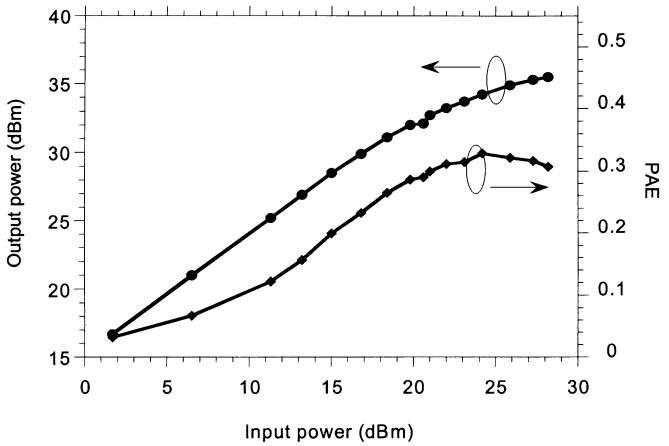

(a)

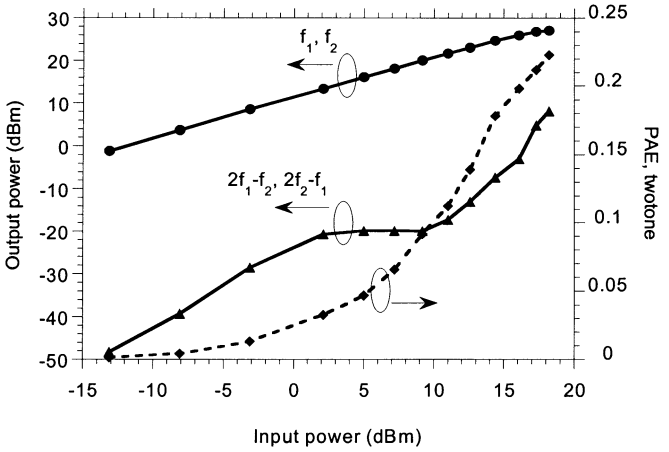

(b)

Fig. 19. Class-B bias common-source power-amplifier measurement data. (a) Single-tone output power and PAE. (b) Two-tone output power and IM3 suppression.

circuits the signal harmonics. The PAE simulations are shown in Fig. 15. In simulations, the circuit produces 36-dBm saturated output power with a maximum PAE of 54% at 5 GHz. This circuit has an IM3 suppression of 45 dBc at output power levels 3 dB below the 1-dB compression point when biased at class B. The bias has been varied from class C to class A, and the IMD performance is plotted in Fig. 16. It is clear that, at 5 GHz, the circuit has low distortion when biased at or above class B. The class-B bias shows 45 dBc of IM3 suppression at 1-GHz operation. At 5 GHz, IM3 suppression is greater than 35 dBc over all biases ranging from class B to class A. This confirms the earlier analysis.

There is superior performance at lower frequencies. However, as the frequency increases, the distortion increases due to the effect of voltage variation of the input capacitance. As is expected from the input capacitance nonlinearity analysis (Section IV), in the high-frequency limit, where $C_{\rm gs}$ nonlinearity dominates, IM3 suppression is best at class-B and class-A bias conditions. Low distortion at higher frequencies can be achieved using HEMTs with smaller gate lengths resulting in increased f_t. With common-drain class-AB amplifier, low distortion could be obtained for signal frequencies $<f_t/10$.

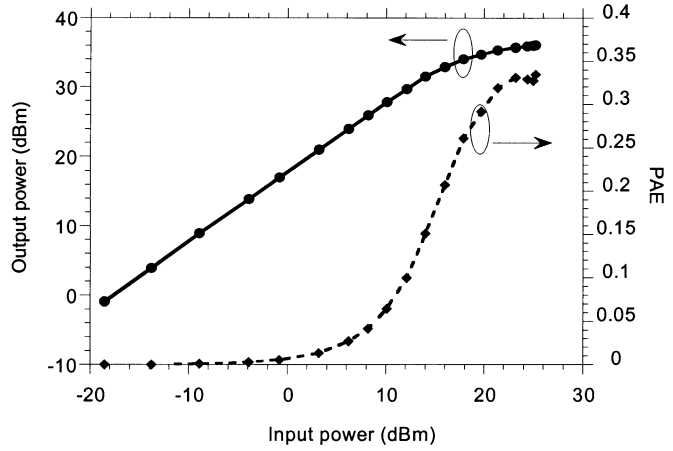

(a)

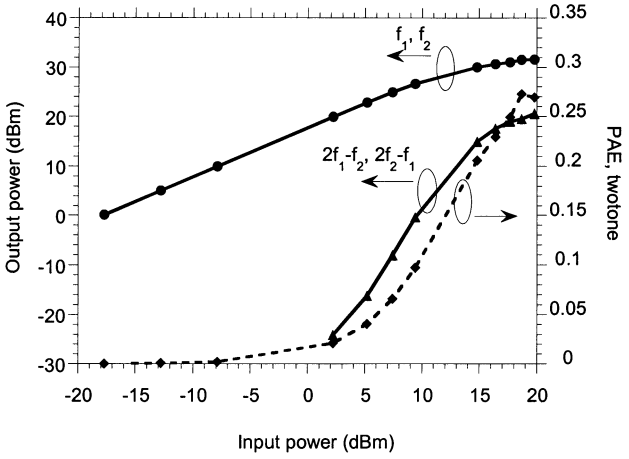

(b)

Fig. 20. Class-A bias power-amplifier measurement data. (a) Single-tone output power and PAE. (b) Two-tone output power and IM3 suppression.

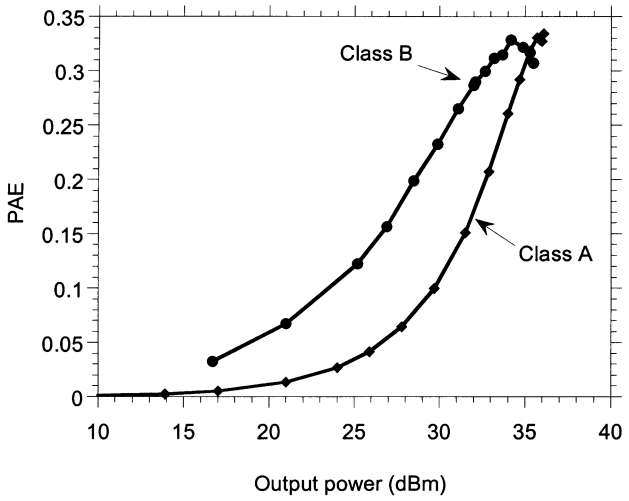

(a)

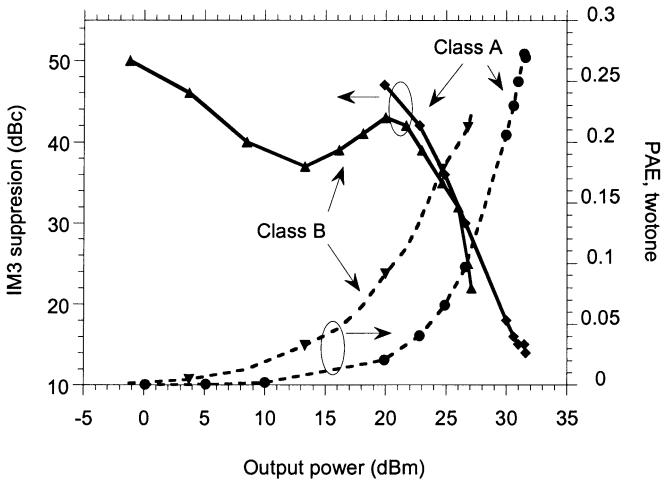

(b)

Fig. 21. Summary of comparison between class-B and class-A data. (a) Single-tone PAE. (b) Two-tone PAE and IM3 suppression.

X. Fabrication and Testing of Common-Source Class B

The MMIC class-B power amplifier is fabricated on an SiC substrate in the GaN HEMT technology (Fig. 17). The 1.2-mm dual-gate GaN HEMT has 1-A/mm $I_{\rm dss}$ and >55-V breakdown voltage. The measured f_t for the 0.25-μm L_g device is 45 GHz. Fabricated devices have $V_{\rm th} = -5.1$ V.

All input and output tuning networks are on-chip. Bias feeds for gate 1, gate 2, and drain were provided through off-wafer bias tees for convenience. The circuit is tested with four different bias conditions, i.e., -3.1 V for class A, -4 V for class AB, -5.1 V for class B, and -5.5 V for class C, respectively. Single- and two-tone measurements were performed. The third-order output powers $2f_1 - f_2$ and $2f_2 - f_1$ are measured with two input signals at $f_1 = 8$ GHz and $f_2 = 8.001$ GHz.

The circuit under class-B bias condition exhibits 13-dB gain at 8 GHz with a 7–10-GHz bandwidth, as shown in Fig. 18. Gain under class-AB or class-A bias conditions was roughly 6 dB greater than in class B, as is expected. 36 dBm of saturated output power and 34% of maximum PAE are obtained at the class-B bias condition for single tone [see Fig. 19(a)], and high IM3 suppression is obtained over a wide output power range for two-tone input signals [see Fig. 19(b)]. Note that the IM3 amplitude does not vary in proportion to the cube of the input power

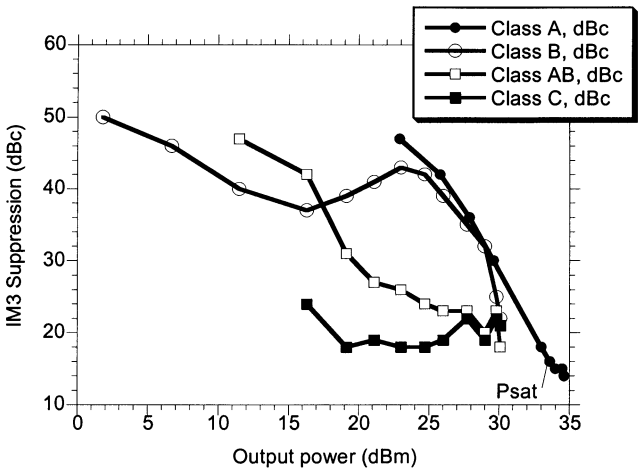

Fig. 22. IM3 suppressions for all bias conditions as a function of output power.

because the circuit transfer characteristics are not well modeled by a cubic polynomial. Device models (Section VII) provide only an approximate fit to the device characteristics and, hence, the discrepancy between simulations (Fig. 11) and measurement

[see Fig. 19(b)]. Under class-A bias, shown in Fig. 20(a) and (b), the IM3 output power increases rapidly with the input power, making IM3 suppression very poor at high output power levels.

Comparison of the PAE and IM3 suppression versus output power for classes A and B are shown in Fig. 21(a) and (b), respectively. At low output power levels, class A has very low distortion (IM3 $>$ 50 dBc), while IM3 suppression of class B also maintains a $>$35-dBc level. At high power levels, however, class B and class A have similar IM3 suppression, but class B provides 10% improved PAE, as can be seen in Fig. 21(b). The IM3 performance versus output power for classes A, AB, B, and C are compared in Fig. 22. Class AB and class C have higher IMD when compared to classes A and B.

XI. Conclusions

For class-B amplifiers with fractional bandwidth less than 2 : 1, the push–pull configuration is unnecessary and can be replaced by a single-ended configuration with output filtering. This avoids the difficulty of fabricating balun transformers with correct harmonic termination at microwave frequencies. If the HEMT transconductance is independent of gate bias above threshold, low IMD3 levels can be attained. The single-ended common-source class-B amplifier has shown more than 35 dBc of IM3 suppression at 8 GHz with approximately 34% PAE. The class-B mode of operation can have a similar distortion level as that of class A if biased right at the pinchoff point, and can yield more than 10% improved PAE over class A. The common-drain class-B power amplifier has low distortion over a wider range of bias due to its integral negative feedback mechanism. This circuit is simulated with 54% of PAE with 45 dBc of IM3 suppression at 5 GHz at the same output power level. The common-drain amplifier is currently being designed and fabricated for future measurement. Combined with the excellent power density of GaN HEMTs, the circuit presented in this paper illustrates the potential of GaN for use in high linearity power amplifiers with good overall efficiency.

Acknowledgment

The authors would like to acknowledge Dr. W. Curtice, Curtice Consulting, Washington Crossing, PA, for providing his HEMT model. The authors also would like to thank L.-Y. Chen, Agile Materials, Santa Barbara, CA, B. Mitchell, University of California at Santa Barbara (UCSB), M. Urteaga, UCSB, L. Shen, UCSB, Y. Wei, UCSB, M. Dahlstrom, UCSB, Z. Griffith, UCSB, D. Scott, UCSB, I. Harrison, University of Nottingham, Nottingham, U.K., N. Parthasarathy, UCSB, J. Yao, UCSB, T. Long, UCSB, and S. Krishnan, Texas Instruments Incorporated, Bangalore, India, for their help.

References

[1] K. Krishnamurthy *et al.*, "Broadband GaAs MESFET and GaN HEMT resistive feedback power amplifiers," *IEEE J. Solid-State Circuits*, vol. 35, pp. 1285–1292, Sept. 2000.

[2] F. H. Raab, "Maximum efficiency and output of class-F power amplifiers," *IEEE Trans. Microwave Theory Tech.*, vol. 49, pp. 1162–1166, June 2001.

[3] H. Kobayashi *et al.*, "Current-mode class-D power amplifiers for high-efficiency RF applications," *IEEE Trans. Microwave Theory Tech.*, vol. 49, pp. 2480–2485, Dec. 2001.

[4] J. R. Shealy *et al.*, "An AlGaN/GaN high-electron-mobility transistor with an AlN sub-buffer layer," *J. Phys., Condensed Matter*, vol. 14, no. 13, pp. 3499–3509, Apr. 2002.

[5] B. M. Green *et al.*, "High-power broad-band AlGaN/GaN HEMT MMIC's on SiC substrates," *IEEE Trans. Microwave Theory Tech.*, vol. 49, pp. 2486–2493, Dec. 2001.

[6] L. Jong-Wook and K. J. Webb *et al.*, "Broad-band GaN HEMT push–pull microwave power amplifier," *IEEE Microwave Wireless Comp. Lett.*, vol. 11, pp. 367–369, Sept. 2001.

[7] N. Vellas *et al.*, "High linearity performances of GaN HEMT devices on silicon substrate at 4 GHz," *IEEE Electron Device Lett.*, vol. 23, pp. 461–463, Aug. 2002.

[8] J. Joseph, "Teaching design while constructing a 100-watt audio amplifier," in *Proc. IEEE Frontiers in Education Conf.*, vol. 1, Nov. 1997, pp. 170–172.

[9] E. E. Zepler, *The Technique of Radio Design*. New York: Wiley, 1943.

[10] H. L. Krauss, W. Bostian, and F. H. Raab, *Solid State Radio Engineering*. New York: Wiley, 1980.

[11] V. Paidi *et al.*, "High linearity and high efficiency of class B power amplifiers in GaN HEMT technology," in *The Lester Eastman Conf.*, Newark, DE, Aug. 2002, pp. 101–107.

[12] K. Krishnamurthy *et al.*, "Dual-gate A1GaN/GaN modulation-doped field-effect transistors with cutoff frequencies $f_t > 60$ GHz," *IEEE Electron Device Lett.*, vol. 21, Dec. 2000.

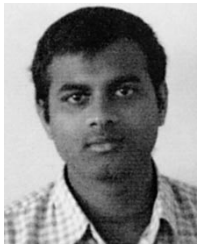

Vamsi Paidi received the B.Tech degree in electrical engineering from the Indian Institute of Technology (IIT), Madras, India, in 2000, and is currently working toward the Ph.D. degree at the University of California at Santa Barbara (UCSB).

His research includes design and fabrication of power amplifiers for wireless applications using GaN HEMTs.

Shouxuan Xie (S'01) was born in Tianjin, China, in 1972. He received the B.S. and M.S. degrees in electrical engineering from the Nankai University, Tianjin, China, in 1995 and 1998, respectively, the M.S. degree in physics from Southern Methodist University, Dallas, TX, in 2000, and is currently working toward the Ph.D. degree in electrical engineering at the University of California at Santa Barbara (UCSB).

His research interests include design and fabrication of highly linear power amplifiers in GaN HEMT technology for wireless communication applications.

Robert Coffie was born in Abilene, TX, in 1974. He received the B.S. degree in engineering physics from the University of Oklahoma, Norman, in 1997, and the M.S. degree in electrical engineering from the University of California at Santa Barbara.

From 1997 to 1999, he was a Product Engineer for GaAs-based pseudomorphic high electron-mobility transistors (pHEMTs), heterostructure field-effect transistors (HFETs), and MESFETs with the Texas Division, TriQuint Semiconductor. His current research is in GaN-based HEMTs.

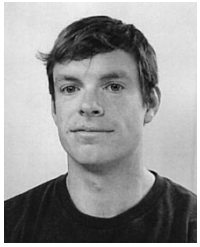

Brendan Moran was born in Teaneck, NJ, in May 1976. He received the B.E. degree in materials science and engineering from The Johns Hopkins University, Baltimore, MD, in 1998, and is currently working toward the Ph.D. degree in materials at the University of California at Santa Barbara.

His research involves the MOCVD growth of GaN on SiC and Si for electronic device applications. His primary interest in this effort is the relationship between structural and point defects on the performance of HEMT devices.

Sten Heikman received the Civilingenjör degree in applied physics and electrical engineering from the Linköping University, Linköping, Sweden, in 1998, the M.S. degree in electrical and computer engineering from the University of Massachusetts, Amherst, in 1998, and the Ph.D. degree in electrical and computer engineering from the University of California at Santa Barbara, in 2002.

He is currently with the Department of Electrical and Computer Engineering, University of California at Santa Barbara, where he conducts research on various aspects of group-III nitride semiconductors, including FET structures and epitaxial growth techniques.

Stacia Keller received the Diploma and Ph.D. degrees in chemistry from the University of Leipzig, Leipzig, Germany, in 1983 and 1986, respectively.

As a Scientific Assistant, she continued her experimental and theoretical work in the field of epitaxial growth of GaAs- and InP-based semiconductors. In 1994, she joined the Electrical and Computer Engineering Department, University of California at Santa Barbara. Her current research interests are the crystal growth and characterization of group-III nitrides for electronic and opto-electronic applications. She has authored or coauthored over 100 technical publications and 90 conference presentations. She holds two patents.

Alessandro Chini was born in Rovereto, Italy, in 1975. He received the Laurea degree in electronic engineering from the University of Padova, Padova, Italy, in 1999, and is currently working toward the Ph.D. degree at the University of Padova.

Since 2001, he has been with the Department of Electrical and Computer Engineering, University of California at Santa Barbara. His current research interests involve the fabrication, characterization, and reliability of GaN-based HEMTs for microwave power applications.

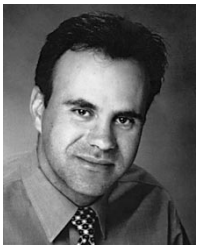

Steven P. DenBaars (M'91) received the M.S. and Ph.D. degrees in electrical engineering from the University of Southern California, Los Angeles, in 1986 and 1988, respectively.

He is currently a Professor of Materials and Electrical Engineering at the University of California at Santa Barbara (UCSB). He is also currently a Co-Director of the Solid State Lighting and Display Center (SSLDC), UCSB, which is developing new and more energy-efficient light sources. His special interests include the effect of materials properties on device performance, blue VCSEL lasers, and microwave power transistors. From 1988 to 1991, he was a Member of the Technical Staff at Hewlett-Packard, where he was involved in the fabrication of high-brightness LEDs. In 1991, he joined the faculty of the UCSB, where he develops new solid-state opto-electronic devices. He has authored over 200 technical publications, three book chapters, and 100 conference presentations. He holds over seven patents. His research also involves MOCVD growth of InP-based tunable lasers and detectors.

Dr. DenBaars was the recipient of the 1995 National Science Foundation Young Scientist Award and the 1998 Young Scientist Award presented at the International Symposium on Compound Semiconductors.

Umesh K. Mishra (S'80–M'83–SM'90–F'95) received the Ph.D. degree from Cornell University, Ithaca, NY, in 1984, the M.S. degree from Lehigh University, Bethlehem, PA, in 1980, and the B.Tech. degree from the Indian Institute of Technology (IIT) Kanpur, India, in 1979, all in electrical engineering.

He has worked in various laboratory and academic institutions, including Hughes Research Laboratories, Malibu, CA, The University of Michigan at Ann Arbor, and General Electric, Syracuse, NY, where he has made major contributions to the development of AlInAs–GaInAs HEMTs and HBTs. He is currently a Professor with the Department of Electrical and Computer Engineering, University of California at Santa Barbara, Santa Barbara. His current research interests are oxide-based III–V electronics and III–V nitride electronics and opto-electronics. He has authored or coauthored over 400 papers in technical journals and conferences. He holds eight patents.

Dr. Mishra was a corecipient of the Hyland Patent Award presented by Hughes Aircraft and the Young Scientist Award presented at the International Symposium on GaAs and Related Compounds.

Stephen Long (S'68–M'73–SM'80) received the B.S. degree in engineering physics from the University of California at Berkeley, in 1967, and the M.S. and Ph.D. degrees in electrical engineering from Cornell University, Ithaca, NY, in 1969 and 1974, respectively.

From 1974 to 1977, he was a Senior Engineer and Manager of Semiconductor Engineering with Varian Associates, Palo Alto, CA. From 1978 to 1981, he was a Member of the Technical Staff with Rockwell International Science Center, Thousand Oaks, CA. In 1981, he joined the Electrical and Computer Engineering Department, University of California at Santa Barbara, where he is currently a Professor. In 1988, he was a Research Visitor at GEC Hirst Research Centre, London, U.K. In 1994, he was a Fulbright Research Visitor with the Signal Processing Laboratory, Tampere University of Technology, Tampere, Finland, and a Visiting Professor with the Electromagnetics Institute, Technical University of Denmark, Lyngby, Denmark. In 1999, he was a Visitor with the Hewlett-Packard HP/EEsof Division, Santa Rosa, CA. His research interests include the design of very high-speed digital ICs, high-performance devices and fabrication technologies, and high-frequency analog ICs for wireless and fiber-optic communications.

Dr. Long was the recipient of the 1978 IEEE Microwave Applications Award for development of InP millimeter-wave devices.

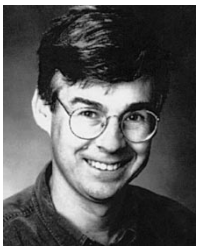

Mark J. W. Rodwell (M'89–SM'99) He has held positions as a Member of the Technical Staff with AT&T Bell Laboratories and as a Research Associate at Stanford University. He is active as a consultant for Hughes Malibu Research Laboratories, where he consults in the areas of radar, microwave integrated-circuit design, and microwave and optical communications systems, and for New Focus Inc., where he consults in the areas of optical links and high-frequency instruments. His interests are in electronics operating in the 1–1000-GHz range. His activities include fabrication processes, semiconductor devices, integrated-circuit design, and instrument and communication system design. His work has been recognized by an Invited Paper in the PROCEEDINGS OF THE IEEE. His current research involves submicrometer scaling of HBTs and development of HBT ICs for analog–digital converters and fiber-optic regenerators. His group has developed record bandwidth HBTs, deep-submicrometer Schottky-collector resonant-tunnel diodes with terahertz bandwidths, and monolithic submillimeter-wave oscillators with these devices. His group has worked extensively in the area of GaAs Schottky-diode ICs for subpicosecond pulse generation, submillimeter-wave signal sampling, and millimeter-wave instrumentation.

Dr. Rodwell was the recipient of the 1997 IEEE Microwave Prize in recognition of the impact of his work on commercial high-end instruments. He was also the recipient of a 1989 National Science Foundation Presidential Young Investigator Award.